The mechanism of deposition of calcium phosphate coatings from solution onto magnesium alloy AZ31

J. E. Gray-Munro, M. Strong
Department of Chemistry and Biochemistry, Laurentian University, Sudbury, Ontario, Canada P3E 2C6

Received 24 September 2007; revised 31 January 2008; accepted 12 February 2008
Published online 28 May 2008 in Wiley InterScience (www.interscience.wiley.com). DOI: 10.1002/jbm.a.32107

Abstract: In recent years, magnesium alloys have been proposed as a new class of metallic bioabsorbable implant material. Unfortunately, hydrogen gas evolution and an increase in alkalinity are both byproducts of the degradation process. This necessitates the development of magnesium alloys with controlled degradation rates. The development of biocompatible coatings that can delay the onset of corrosion is essential for improving the lifetime and performance of these materials *in vivo*. Calcium phosphate coatings have been shown to improve the biocompatibility of metallic implants for orthopedic applications. In this article, we report a solution chemistry technique for depositing calcium phosphate coatings on magnesium alloy surfaces. Our kinetic studies indicate that the deposition of the coating is related to the anodic dissolution of the substrate. Characterization of the coating by XPS, SEM/EDS, and XRD reveal that the coating produced is a poorly crystalline calcium magnesium hydroxyapatite material. © 2008 Wiley Periodicals, Inc. J Biomed Mater Res 90A: 339–350, 2009

Key words: calcium phosphate coating; magnesium; hydroxyapatite; surface analysis

INTRODUCTION

Bioabsorbable materials are desirable for a wide variety of clinical applications including fracture fixation, orthopedic surgery, endovascular stents, and controlled drug delivery systems.[1–3] The use of bioabsorbable materials in orthopedics is of particular interest, because in many instances, the implant serves no function as soon as healing and union of the tissue has occurred.[2] These implants are typically fabricated from bioinert materials such as titanium or stainless steel and they are only truly necessary for a 3- to 6-month period, but in order to remove them, the patient would have to undergo a second surgery.[1] This is both costly and can pose a serious health risk for the patient. Another possible course of action is to simply leave the implant in place. This also has disadvantages including corrosion of the implant *in vivo*, stress-protection weakening of the surrounding bone, and development of allergic reactions to metals.[1–3] The use of a bioabsorbable implant would effectively avoid all of these problems. The implant would provide the necessary stability in the initial stages of healing and would gradually be replaced with bone as it degraded.[1–3]

Unfortunately, the biobsorbable polymeric materials that are currently in use have been shown to have less than ideal biocompatibility.[1,3] The development of magnesium alloy implant materials is a novel approach to overcome the current drawbacks associated with both traditional metallic implant materials and polymeric bioabsorbable materials. Magnesium and its alloys have a number of advantages over traditional metallic biomaterials, such as their high strength to weight ratio, inherent biocompatibility, and mechanical properties that are similar to bone.[4] Unfortunately, magnesium also has extremely poor corrosion resistance, particularly in the presence of chloride ions[5–7]; this has limited its use as a metallic biomaterial for permanent implants. Magnesium-based metals corrode according to the following general reaction scheme:

$$Mg^0 \rightarrow Mg^{2+} + 2e^-$$

$$2H_2O + 2e^- \rightarrow H_2 \uparrow + 2OH^-$$

However, this susceptibility to corrosion can be seen as a distinct advantage when considering

Correspondence to: J. E. Gray-Munro; e-mail: jgray@laurentian.ca

Contract grant sponsor: Natural Sciences and Engineering Research Council
Contract grant sponsor: Canada Foundation for Innovation
Contract grant sponsor: Laurentian University Research Fund

potential materials for biodegradable implants. Furthermore, it has been demonstrated that magnesium ions have a very positive effect on both cellular adhesion and cellular differentiation of human-derived bone cells on an alumina substrate.[8] It is therefore possible that the release of magnesium ions during the biodegradation of the alloy will result in improved cell/surface interactions compared to traditional polymeric biodegradable materials. Preliminary cytotoxicity tests have also indicated that magnesium had no inhibitory effects on marrow cell growth[9] and that these materials have good biocompatibility.[10–13] It has even been demonstrated that magnesium alloys may have antibacterial properties.[14] This would be an added feature for the prevention of bacterial biofilm formation on the surface of these implants.

To date, there are relatively few publications describing magnesium alloys as a biomaterial. Preliminary *in vivo* animal studies have demonstrated that a magnesium alloy implanted in the femura of guinea pigs was completely replaced by new bone formation within 18 weeks[7,15] and that magnesium-based alloys may be a promising material for cardiovascular applications.[10,16–17] Bone remodeling around open-porous magnesium alloy scaffolds has also been observed.[12]

Unfortunately, hydrogen gas evolution and an increase in alkalinity are both byproducts of the corrosion reaction. However, a study by Witte et al. showed that subcutaneous gas bubbles were formed in the first 2–3 weeks of magnesium alloy implantation (in guinea pigs) and then disappeared.[15] The gas bubbles were readily removed by puncturing with a syringe, and no adverse effects were observed in the guinea pigs.[15] This demonstrates that if the corrosion rate can be controlled, the hydrogen gas generated should not be a problem. Therefore, the development of biocompatible coatings that can delay the onset of corrosion is essential to the successful development of magnesium alloy implants. It has been demonstrated that surface treatment by alkali heat treatment,[18] anodizing,[19] and titanium ion implantation[20] may have a positive impact on the corrosion rate of magnesium alloy materials in simulated biological fluid (SBF).

The main mineral component of bone is calcium-deficient carbonate hydroxyapatite.[21] Calcium phosphate coatings have been shown to improve the biocompatibility of metallic implants and to increase bone growth at the site of implantation.[22,23] In particular, biomimetically deposited coatings have received recent attention because of their excellent biocompatibility and ability to promote osseointegration.[24–27]

The biomimetic approach is a solution technique that involves immersing the substrate material in SBF at low (ambient to physiological) temperatures. This technique has been successfully used to apply calcium phosphate coatings onto various substrates.[25] This type of approach is advantageous when compared to the more widely used plasma spraying for a number of reasons:

1. It is a low-temperature process that does not alter the substrate significantly and can be used to coprecipitate biological molecules such as proteins and growth factors.[24]
2. Bone-like apatite crystals having high bioactivity and good resorption characteristics can be deposited.[25]
3. Implants with complex or porous geometries can be uniformly coated.

The composition of the coating bath and the chemistry of the implant surface have both been shown to play a key role in the nucleation and growth of calcium phosphate coatings from SBF. The Ca/P ratio, presence of inorganic ions such as Mg^{2+}, surface pretreatment, and coating post-treatment have all been shown to have a significant influence on the deposition rate and type of calcium phosphate phase deposited on implant materials.[28–34]

Although the precipitation of calcium phosphates on magnesium alloys has been observed during both *in vitro* and *in vivo* corrosion studies of magnesium alloys,[4,15,18,35] there are no reports of the development of calcium phosphate coatings for these materials. In this article, an aqueous phase coating process for depositing calcium phosphate coatings on magnesium alloy AZ31 has been reported. The mechanism of deposition has also been explored. AZ31 was chosen for this study for three reasons: (1) it contains a relatively small amount of potentially toxic aluminium, (2) its mechanical properties have been shown to be a good match to bone,[4] and (3) it has been shown to degrade *in vivo* at a similar rate as AZ91 and WE43.[15] This makes it an optimum choice because AZ91 contains more aluminium, and WE43 contains several rare earth elements that are known to have moderate toxicity.

EXPERIMENTAL DETAILS

Pretreatment of magnesium alloy substrates

Magnesium aluminium zinc foil (2 cm × 1 cm coupons; Alfa Aesar) with a composition of 96%Mg:3%Al:1%Zn by weight were ultrasonically cleaned in trichloroethylene (Baker analyzed reagent grade) for 30 min at room temperature in a Bransonic 220 sonicator and subsequently rinsed with distilled water. The samples were then ultrasonically cleaned in a sodium carbonate monohydrate solution (25 g/L) for 30 min at 50°C in a Transsonic Digital S sonicator. The samples were then rinsed thoroughly with distilled

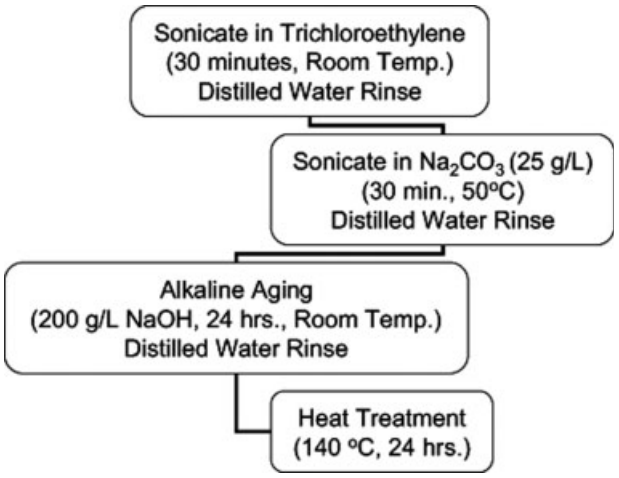

Figure 1. Pretreatment scheme.

water. Subsequent pretreatment procedures include alkaline aging in a 200 g/L sodium hydroxide solution (Aldrich) followed by heat treatment for 24 h at 140°C. Alkaline aging was used to increase the surface concentration of hydroxyl groups. This has been shown to be effective in inducing calcium phosphate deposition from aqueous solutions on other materials such as titanium and stainless steel.[31] The overall pretreatment scheme is illustrated in Figure 1.

Deposition of calcium phosphate coatings

Calcium phosphate solutions were prepared in a 1.67:1 calcium: phosphate ratio (the stoichiometric ratio of hydroxyapatite) unless otherwise specified. The composition of the coating bath was 3.0 m*M* $CaCl_2$ and 1.8 m*M* Na_2HPO_4. These concentrations were chosen in order to obtain a saturated solution. The pH of the solution was adjusted to 5 with a dilute solution of hydrochloric acid. This pH was chosen because our preliminary results indicated that the best calcium phosphate coatings were obtained under mildly acidic conditions. The magnesium alloy coupons were immersed in 250 mL of the calcium phosphate bath for a predetermined period of time from a few minutes to 1 week. Upon removal from the coating bath, the samples were immediately air-dried.

Monitoring of the solution chemistry during coating deposition

The concentrations of magnesium, calcium, and phosphorus in the coating bath were monitored as a function of coating deposition time. This was achieved by taking small aliquots from the coating bath hourly for the first 3 h of immersion in the bath and subsequently at 24-h time intervals. The samples were then analyzed quantitatively for magnesium and calcium by flame atomic absorption spectroscopy and by high-performance liquid chromatography for phosphate.

Aqueous magnesium and calcium concentrations by flame atomic absorption spectroscopy

For the first 3 h of immersion, 200-μL aliquots were taken and diluted up to 25 mL using 2% v/v nitric acid. The remaining aliquots were taken in 24-h time intervals (50 μL diluted up to 25mL using 2%v/v nitric acid). The samples were immediately placed in a refrigerator to prevent volume changes. All aqueous magnesium and calcium determinations were done using a Perkin-Elmer 5000 flame atomic spectrophotometer. For magnesium determinations, a wavelength of 285.5 nm was used with a current of 5 mA, for calcium these parameters were 422.7 nm and 5 mA, respectively. Optimal flame conditions were achieved using a C_2H_2/air ratio of 30/40, the scan time was 0.5 s.

Determination of aqueous phosphate concentrations By HPLC

Aliquots for these determinations were taken in a similar manner as for the magnesium and calcium experiments with distilled water as a solvent. The aliquots were diluted 50-fold and 10-fold, respectively, for the aliquots taken within the first 3 h and subsequent samples. All analyses were taken using a Dionex DX 500 chromatography system using 12 m*M* Na_2CO_3 to 5 m*M* $NaHCO_3$ as an eluent with a flow rate of 1.00 mL/min. The current and conductivity were set at 100 mA and 100 μS, respectively. The pump pressure was maintained below 3000 psi for all analyses.

Coating characterization

The composition of the calcium phosphate coating obtained was characterized by X-ray diffraction (XRD), energy-dispersive spectroscopy (EDS), X-ray photoelectron spectroscopy (XPS), and atttenuated total reflection–Fourier transform infrared spectroscopy (ATR-FTIR). The morphology of the coatings was examined by scanning electron microscopy (SEM).

XRD analysis

The coating was removed from the substrate and was investigated using a Debye-Scherrer camera to record data on an image plate. Subsequently, the recorded diffraction pattern was integrated, cumulating the recorded intensities on a 2θ-scale. The 2θ resolution is on the order of ~0.1°. The higher order diffraction data is not reported due to the limitations of the technique and the poor crystallinity of the sample (the higher order peaks were not well defined). The phase(s) were identified using CRYSTALLOGRAPHICA Search/Match. The experimental conditions were 40 kV, 30 mA, and collimator 0.5 mm. The exposure time was incrementally increased, and the best result was achieved after 12 h of exposure.

TABLE I
Approximate Rates of Change for the Concentrations of Relevant Ions in Solution in the Early and Late Stages of Deposition

Ionic Species	Approximate Rate of Change (M/min)	
	Early Stages of Deposition	Later Stages of Deposition
Ca^{2+}	-2.0×10^{-6}	-1.0×10^{-7}
PO_4^{3-}	-8.0×10^{-7}	-6.0×10^{-9}
Mg^{2+}	1.0×10^{-6}	2.0×10^{-7}

XPS analysis

XPS spectra were recorded with a Kratos Axis Ultra X-ray photoeletron spectrometer. The XPS was performed in vacuum at 1×10^{-9} Torr with a take off angle of 90°. The survey scans were recorded over a spot size of 1000 μm between 0 and 1000 eV, and the high-resolution spectra was recorded over an area of 300 × 700 μm with a pass energy of 20 eV. All high-resolution spectra were charged corrected to the C—C in the C(1s) spectrum at 285.0 eV.

FTIR analysis

FTIR spectra were collected using a Bruker Optics Tensor 27 spectrometer. The resolution of the spectrometer was 4 cm^{-1}. Each spectrum is the result of 1000 scans. The spectrometer was equipped with a MCT detector that was liquid nitrogen cooled. The spectra were corrected for CO_2 and H_2O with the atmospheric compensation function of the software.

SEM/EDS analysis

Samples to be analyzed were sputter-coated with a thin film of carbon to render the sample conductive. All samples were analyzed in the Zeiss EVO50 SEM, EDS spectrometer. The vacuum in the chamber was 1.14×10^{-6} mbar. The beam current of the electron gun was set at 1.0 nA. A spot size of 520 nm was used with a working distance of 8.5–9 mm. The collection time for the EDS was set for 45 s.

RESULTS AND DISCUSSION

Time course of the reaction for calcium phosphate deposition

The kinetics of deposition of the calcium phosphate coating on the magnesium alloy surface has been studied by monitoring both the changes in solution chemistry of the coating bath and changes in the surface chemistry of the coating itself as a function of immersion time in the bath.

Solution chemistry

The approximate rates of change for the concentrations of each of the relavent species in the early and late stages of deposition are listed in Table I. The reaction has been divided into early and late stages to illustrate that the reaction slows as the substrate becomes coated with the calcium phosphate film. In the first 12–24 h, the rate of calcium deposition/magnesium dissolution is an order of magnitude higher than the rates observed at later deposition times. The fact that the respective rates seem to follow each other may indicate that the anodic dissolution of magnesium is the catalyst for calcium phosphate deposition.

The change in the concentration of Ca^{2+} ions, PO_4^{3-} ions, and Mg^{2+} ions in the coating bath during deposition is shown in Figure 2. A steep drop in the calcium concentration in the bath is observed in the first 12 h of deposition. This steep deposition rate is followed by a moderate deposition rate up to about 96 h that is an order of magnitude less than the initial rate. Finally, the concentration of calcium ions in the bath levels off. A steep decrease in the aqueous phosphate concentration is also observed in the first 24 h of deposition. This is followed by a very slow decrease in phosphate concentration up to about 96 h, after which no further change in phosphate concentration is observed. A rise in the concentration of magnesium ions in the bath is also observed (there is no magnesium present in the coating bath initially). This increase in magnesium concentration has the steepest slope in the first 12 h of deposition. This steep rise is followed by a moderate increase in magnesium concentration for the rest of the coating process. This increase in magnesium ion concentration is also coupled with a sharp rise in solution pH in

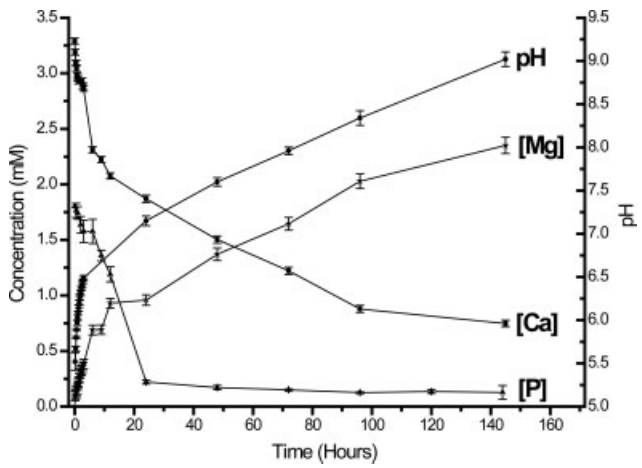

Figure 2. Solution concentration of relevant ions and change in pH during coating deposition.

the first 12 h of deposition, with a subsequent moderate rise in pH until the end of the coating process.

The increase in magnesium ion concentration and pH in the bath can both be attributed to anodic dissolution of the alloy in the coating bath. It is well known that magnesium metal is unstable in aqueous solution at pH values less than 11.[36] Our coating bath has an initial pH value of 5. This is necessary in order to prevent homogeneous nucleation and growth of calcium phosphate crystals in solution. At higher pH, the solutions are unstable and calcium phosphate crystals precipitate rapidly from solution, eliminating the potential for heterogeneous nucleation of calcium phosphate coatings on the magnesium substrates. Upon immersion in the coating bath, an increase in magnesium ions, pH and bubbling are all observed. This can be explained with the following half reactions.

$$Mg^0 \rightarrow Mg^{2+} + 2e^- \quad (1)$$

$$2H_2O + 2e^- \rightarrow H_2 \uparrow + 2OH^- \quad (2)$$

The first reaction is the anodic dissolution of the magnesium metal according to reaction 1, and this is the source of the observed increase in magnesium. The second reaction is the reduction of water to give hydrogen gas, the observed bubbles, and hydroxyl ions which are responsible for the observed rise in pH.

This rise in pH also has an effect on the phosphate species in the coating bath. The following equilibrium [Eq. (3)] represents the species present as a function of pH. The acid dissociation constants for the three equilibria are $pK_1 = 2.14$, $pK_2 = 6.87$ and $pK_3 = 12.32$.[37]

$$H_3PO_4 \leftrightarrow H_2PO_4^- \leftrightarrow HPO_4^{2-} \leftrightarrow PO_4^{3-} \quad (3)$$

This means that at our initial pH of 5 the dominant form of phosphate in the coating bath is $H_2PO_4^-$, as the pH rises to seven the dominant species is mixed $H_2PO_4^-$ and HPO_4^- and at a pH of 9 (the final pH of the bath) the dominant species in solution is HPO_4^-. The pH that we have measured is the bulk pH of the solution, however, because of the reduction of water at the magnesium coupon/coating bath interface, it is likely that the local pH at the interface is substantially higher than the measured pH of the bulk. This opens up the possibility of the PO_4^{3-} phosphate species dominating at this interface.

The initial steep decrease in calcium and phosphate ion concentration in the coating bath indicates that the calcium phosphate coating begins to form immediately upon immersion in the coating bath. No homogeneous (solution) precipitation of calcium phosphate is observed in the early stage of deposition. The decrease in Ca^{2+} and PO_4^{3-} concentration in the early stages of deposition must therefore be due to heterogeneous nucleation and growth of calcium phosphate on the magnesium surface. As the pH of the coating bath rises to approximately pH = 7.5 or after 48 h, calcium phosphate crystals are observed in the bulk of the solution.

For all the solution species monitored, there is a large rate of change in the initial stages of deposition followed by a more moderate rate of change after 12–24 h. The decrease in the rate of magnesium and hydroxyl ion production is due to the formation of the coating itself. As the film thickness and uniformity increases, it acts to passivate the surface from further corrosion to a small extent. However, even at long coating times the magnesium corrosion continues, albeit at a slower rate. The calcium phosphate layer slows the diffusion of water and ions to the surface of the sample thus reducing the corrosion rate. However, the poorly crystalline nature of the coating (contributes to dissolution of the coating in the bath) and the presence of small defects (cracks or pores) means that aqueous ions can still diffuse in and out of the coating. The anodic dissolution of the magnesium substrate thus continues.

The change in the rate of consumption of calcium and phosphate ions is likely due to a combination of two main factors. The first factor is the depletion of reactants as the reaction proceeds. The initial coating bath is supersaturated with calcium and phosphate.

As the reaction proceeds, the coating bath becomes more dilute in these two ions, and therefore the solubility of the calcium phosphate increases resulting in less deposition. Furthermore, the decrease in the corrosion rate due to passivation of the surface by the coating results in a lower pH at the interface and an increase in the solubility of the calcium phosphate salts.

The second factor that may contribute to an apparent decrease in the rate of calcium and phosphate consumption is the dissolution of the coating in the coating bath. In particular, a net dissolution of amorphous hydroxyapatite phases in SBF has been shown to occur, particularly in the early stages of immersion in these solutions.[38,39]

In the final stages of deposition, the concentrations of calcium and phosphate ions both level off indicating no further deposition of calcium phosphate, most likely due to depletion of these ions to a level well below supersaturation.

Surface chemistry

SEM studies

SEM images showing the morphology of the coatings as a function of immersion time in the coating

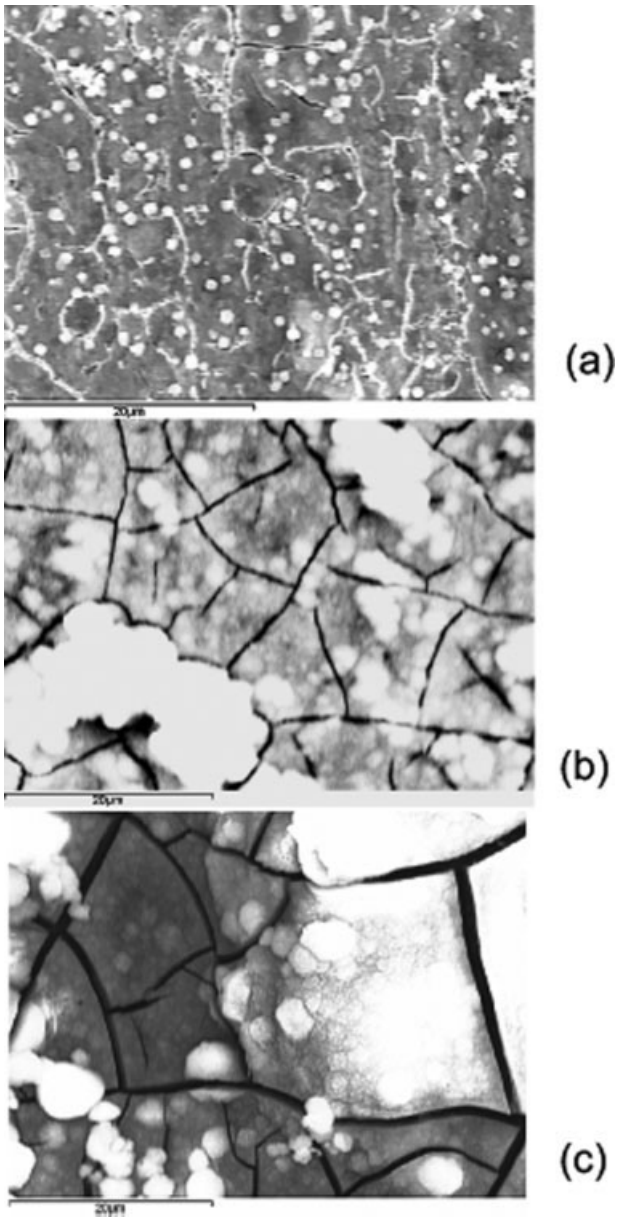

Figure 3. Scanning electron microscopy images of calcium phosphate coatings on magnesium AZ31 substrates at various deposition times. (a) 3 h, (b) 24 h, (c) 96 h.

bath are shown in Figure 3. It is immediately obvious from these images that as the immersion time in the bath increases from 3 h [Fig. 3(a)] to 24 h [Fig. 3(b)] and finally to 96 h [Fig. 3(c)] the film thickness also increases. Chemical analysis by EDS confirms this assertion, since the calcium/magnesium ratio increases from 0.087 at 3 h to 1.49 after 24 h and finally to 19.31 after 96 h in the coating bath, indicating an increase in the amount of calcium at the surface as a function of deposition time. This increase in calcium at the surface corresponds directly with the observed decrease in the concentration of calcium ions in the coating bath solution. Figure 3(a) shows the SEM image of the magnesium alloy surface after a relatively short immersion time in the bath. This image shows spherical deposits of calcium phosphate that seem to be localized around small cracks at the surface of the substrate. The observed cracks are due to corrosion of the substrate. As discussed previously, the anodic dissolution of magnesium is coupled with the reduction of water. This produces hydroxyl ions at the liquid/solid interface leading to a localized high pH and subsequent precipitation of calcium phosphate at the magnesium alloy surface. As the immersion time increases, the calcium phosphate spheres grow and begin to precipitate on all areas of the magnesium alloy surface until they coalesce, and a continuous calcium phosphate film is achieved as seen in Figure 3(b). The visible cracks in the calcium phosphate film are likely due to dehydration of the film. At even longer immersion times, additional layers of calcium phosphate deposit on top of the initially formed calcium phosphate layer [Fig. 3(c)].

One important point to note is that the presence of magnesium is observed by EDS even at long coating times and for relatively thick coatings. This suggests that magnesium is present in the coating; however, the sampling depth for EDS is on the order of 3–4 μm. Therefore, our EDS results cannot conclusively determine if the magnesium is present in the coating itself or part of the substrate.

XPS studies

XPS is a surface sensitive technique that probes the first 5–10 nm of the sample surface. From our SEM results, it is obvious that by a 24-h immersion time the coating thickness has exceeded the sampling depth of XPS.

Figure 4 shows survey scans for a magnesium coupon before and after immersion in the calcium phosphate bath for 120 h. Even at the longest coating times, magnesium is still detected on the surface of the coated substrates. This confirms that the magnesium must be incorporated into the calcium phosphate coating since the coating thickness for these samples is much greater than 5–10 nm.

Figure 5 shows a graph of the Ca/Mg ratio as a function of immersion time. The corresponding changes in Mg/C ratio are shown in Figure 6(c). There is an initial increase in the Ca/Mg ratio coupled with a decrease in the Mg/C ratio up to a 6-h immersion time in the bath. These two observations can both be attributed to an increase in film thickness up to this point. As the immersion time increases beyond 6 h there is a decrease in the surface Ca/Mg ratio and a very slight increase in the Mg/C ratio. This can be attributed to a combination of two factors. The first is that the film thickness has

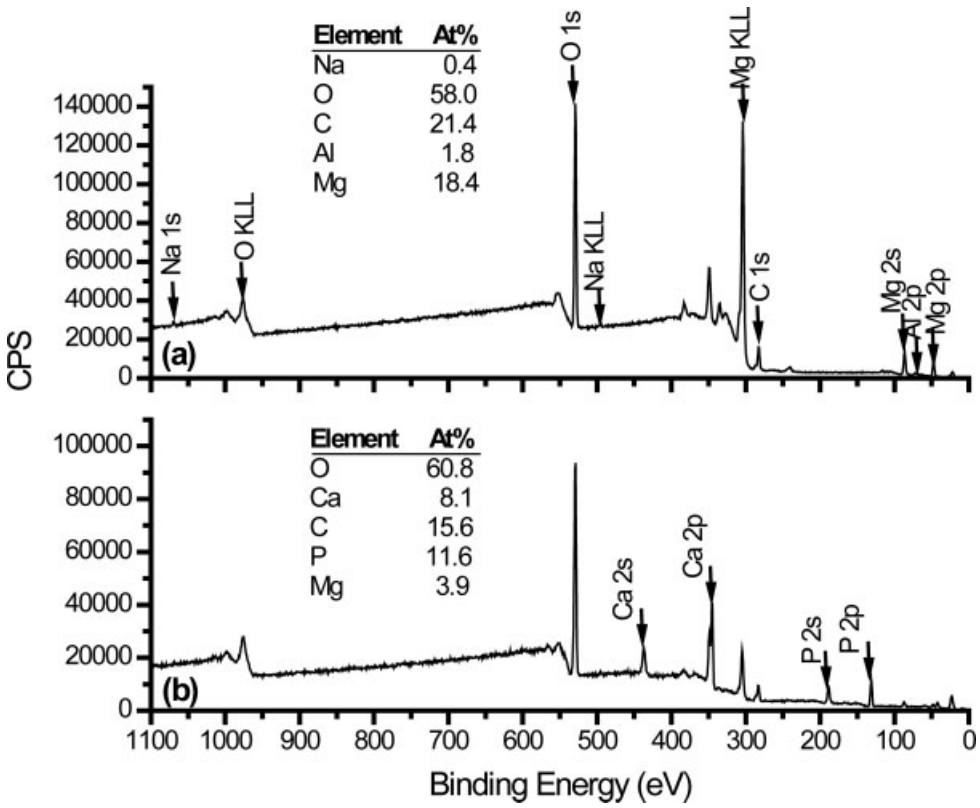

Figure 4. XPS survey scans of calcium phosphate coating on magnesium AZ31 substrates before and after immersion in the coating bath for 5 days. (a) Before immersion in the bath and (b) after immersion in the bath for 5 days.

exceeded the sampling depth of the technique beyond 6 h of immersion in the coating bath. This would be expected to result in a leveling off of the Ca/Mg ratio and a drop to zero for the Mg/C ratio. The observed decrease in the Ca/Mg ratio and slight increase in Mg/C ratio implies an increase in surface magnesium concentration however we know that the substrate is completely covered with the calcium phosphate film at the longer immersion times (Fig. 3) so we are no longer probing the sample substrate. This observation can therefore be attributed to a combination of two factors: (1) incorporation of magnesium ions, from the corrosion of the alloy, into the coating and (2) magnesium ions adsorbing to the surface from solution.

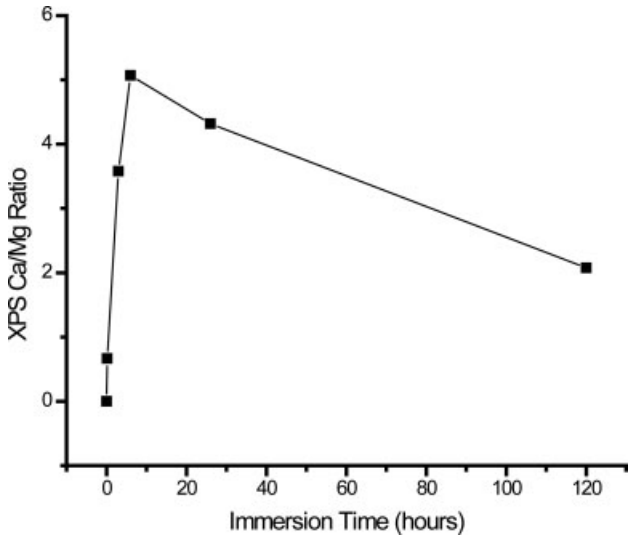

Figure 5. XPS Ca/Mg ratio as a function of coating deposition time.

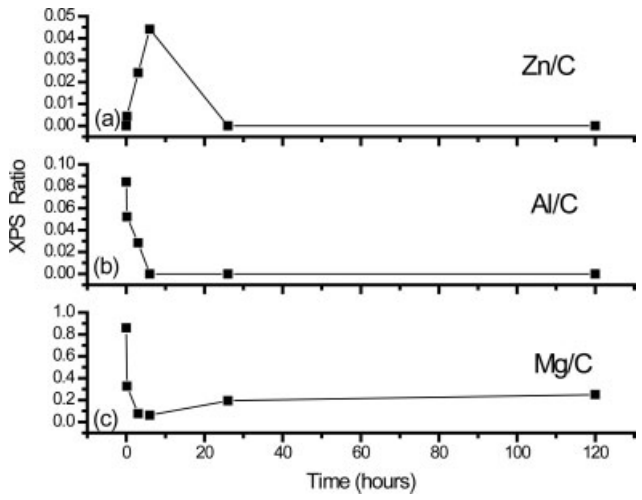

Figure 6. XPS ratios as a function of coating deposition time. (a) Zn/C, (b) Al/C, (c) Mg/C.

Figure 6 also shows the Zn/C and Al/C XPS ratios for the coated samples as a function of immersion time in the calcium phosphate bath. The carbon in the XPS spectra is adventitious carbon from the atmosphere. It is commonly used as an internal reference since it is present on all samples. This figure has two interesting trends. The first is that the surface concentration of aluminum steadily decreases, until at 6 h of immersion time it is no longer detected [Fig. 6(a)]. Since aluminum is mainly present in the substrate, this confirms that by an immersion time of 6 h in the coating bath the substrate is covered by a coating greater than 5–10 nm in thickness. The second interesting observation is that the surface concentration of zinc increases up to an immersion time of 6 h and then drops to zero as the immersion time is increased [Fig. 6(b)]. Although the magnesium alloy substrates contains ~1% zinc, the XPS survey scan for the control sample indicates that the concentration of zinc at the surface of the alloy is below the detection limit of the technique. This is likely due to the presence of a passive oxide/hydroxide layer that forms at the surface of these alloys in air or highly basic solutions. Upon immersion in the coating bath, the passive layer is disrupted and corrosion occurs. Bulk magnesium alloy AZ31 has a two-phase microstructure that consists of a magnesium-rich matrix (α phase) and an aluminium-rich intermetallic species, $Mg_{17}Al_{12}$ (β phase) that is precipitated along the grain boundaries.[40] The zinc in the alloy is known to be dissolved primarily within the β phase of the material.[40] Localized corrosion of these alloys has been shown to initiate at the interface between these two phases due to galvanic coupling.[36] Under these conditions, the magnesium-rich phase acts as an anode while the aluminium-rich phase acts as the cathode. The increase in the concentration of zinc is a result of an initial localized corrosion at these sites. As the anodic dissolution of the magnesium proceeds, the reduction of water occurs near the β phase of the material resulting in a local high pH at the interface of the α and β phases of the material. It is therefore likely that calcium phosphate deposition begins in these regions. In fact, our SEM image for the lower deposition time of 3 h [Fig. 3(a)] does show an increase in calcium phosphate at cracks caused by the corrosion process.

By an immersion time of 24 h, the substrate is completely covered with calcium phosphate, and the overall corrosion rate has slowed due to the presence of the calcium phosphate coating and the increased pH of the coating bath. At this point, no zinc is detected on the surface of the coating. In the case of the magnesium ions in solution, we observed a slight increase in surface magnesium at higher immersion times which we attributed to its incorporation into the coating and adsorption to the surface. We do not see this same effect with zinc. This implies that the zinc that is released into solution due to the corrosion of the substrate is incorporated back into the calcium phosphate coating in the early stages of deposition rather than remaining in the aqueous phase. The fact that there is no evidence of either aluminium or zinc adsorption to the surface of these coatings at higher immersion times even though the corrosion must continue, as evidenced by the continued increase in the amount of magnesium in the bath (Fig. 2), may indicate that at longer immersion times the β-phase becomes passivated while the magnesium-rich α-phase continues to corrode.

Coating characterization

In order to confirm the composition and phase of the calcium phosphate coatings the films were characterized by a combination of high-resolution XPS, infrared spectroscopy, and XRD. The XPS spectra were obtained on the as-coated magnesium alloy coupons. In order to perform the infrared and XRD analysis, the coating was carefully removed from the substrate prior to analysis.

High-resolution XPS

Both the SEM/EDS and XPS survey scans indicate that substrate ions are incorporated into the calcium phosphate coating itself during deposition. Our high-resolution XPS spectra (Table II) indicate that there is an increase to higher binding energy for both the Mg 2p and Al 2p peaks after immersion in the coating bath compared to the bare substrate. Initially, the Mg 2p peak occurs at a binding energy of 49.8 eV. This is consistent with the presence of $Mg(OH)_2$[41] and is not surprising since our pretreatment procedure includes soaking the magnesium alloy coupons in a sodium hydroxide solution to promote the formation of surface hydroxyl groups. An increase in surface hydroxyl groups has been previously shown to promote calcium phosphate nucleation and growth on titanium substrates.[31] Af-

TABLE II
XPS Binding Energies for the Selected Elements Before and After Immersion in the Coating Bath

Peak	Binding Energy in Coating Bath (eV)	
	Before Immersion	After Immersion
Mg 2p	49.8	50.5
Al 2p	74.5	75.1
Ca 2p	N/A	347.6
P 2p	N/A	133.4

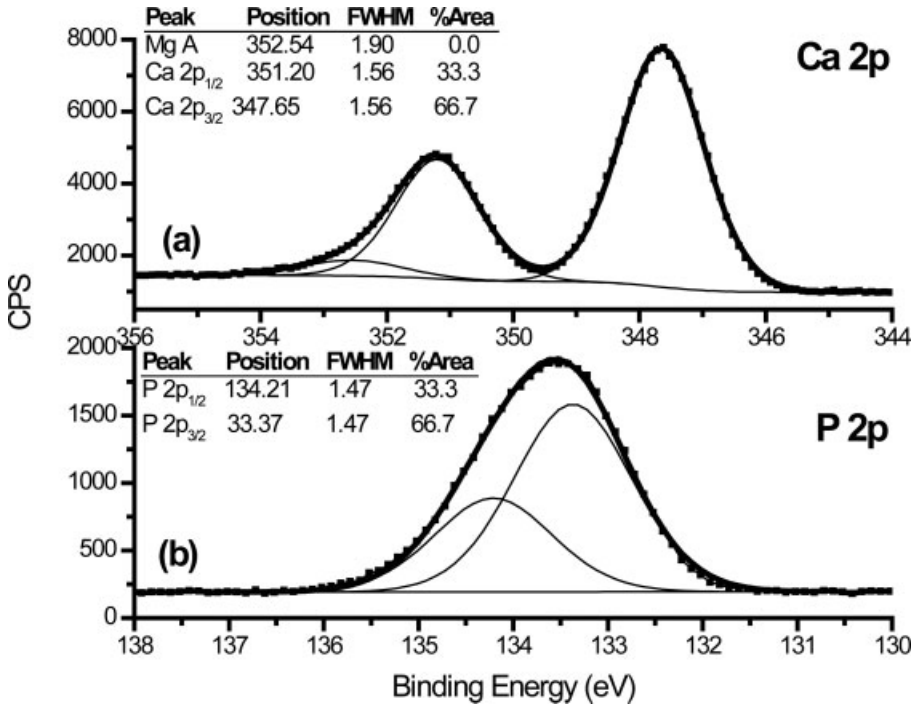

Figure 7. High-resolution XPS spectra for the final calcium phosphate coating. (a) Ca 2p, (b) P 2p.

ter immersion in the coating bath, the Mg 2p peak shifts by 0.7 eV to higher binding energy. The Al 2p peak on the uncoated substrate occurs at a binding energy of 74.5 eV. After immersion in the coating bath, this peak shifts by 0.6 eV to higher binding energy. The binding energy prior to immersion in the coating bath is consistent with aluminium oxide/hydroxide compounds.[42] The shift to higher binding energy for both of these elements supports our assumption that these ions become incorporated into the calcium phosphate coating since both the Mg 2p peak of magnesium phosphate and the Al 2p peak of aluminium phosphate have been shown to have higher binding energies than the corresponding oxide/hydroxides.[42,43]

High-resolution XPS spectra for the Ca 2p and P 2p peaks of the calcium phosphate coating are shown in Figure 7. The Ca 2p peak [Fig. 7(a)] has been deconvoluted into three peaks, consisting of the magnesium auger peak at 352.54 eV, the Ca $2p_{1/2}$ peak at 351.20 eV, and the Ca $2p_{3/2}$ peak at 347.65. The P 2p peak [Fig. 7(b)] has been deconvoluted into two peaks: the P $2p_{1/2}$ peak at 134.21 eV and the P $2p_{3/2}$ peak at 133.37 eV. The binding energies of these peaks are consistent with the reported binding energies for Ca 2p and P 2p in hydroxyapatite.[44] However, it is not possible to differentiate between hydroxyapatite and other calcium phosphate phases on the basis of XPS binding energies alone, since the binding energies for these elements do not shift significantly for other calcium phosphate compounds.[44]

Infrared analysis

Figure 8 shows a representative infrared spectrum of the calcium phosphate coating obtained. The main peaks of interest are annotated on the spectrum. Overall, this spectrum is consistent with the infrared spectrum for hydroxyapatite.[45–47] The sharp peak at 3695 cm^{-1} is the OH stretching vibration for $Mg(OH)_2$[45]. The compound is present at the surface of the sample substrate and is introduced into the coating sample during the removal of the coating from the substrate. Additionally, there is a broad peak centered at 3424 cm^{-1}. This peak has two obvious shoulders; one at 3551 cm^{-1} and the other at ~3300 cm^{-1}. The higher wavenumber shoulder at 3551 cm^{-1} is indicative of the OH stretch for hydroxyapatite[45] while the lower wavenumber shoulder at 3300 cm^{-1} is consistent with the OH stretch for $CaZn_2(PO_4)_2(2H_2O)$ or scholzite.[48] The presence of this compound will be confirmed in the XRD pattern in the next section. The main peak at 3424 cm^{-1} and the peak at 1631 cm^{-1} are due to the OH stretch and bending mode for intercalated water, respectively.[45] The two peaks at 1452 and 1493 cm^{-1} are due to the presence of carbonate ions in the hydroxyapatite structure. It is well known that carbonate, generated from reaction of atmospheric CO_2 with aqueous solutions, readily substitutes for phosphate ions in the crystal structure of hydroxyapatite. Finally, a P—OH band is observed at 869 cm^{-1} as well as three bands at 562, 603, and 1047 cm^{-1}

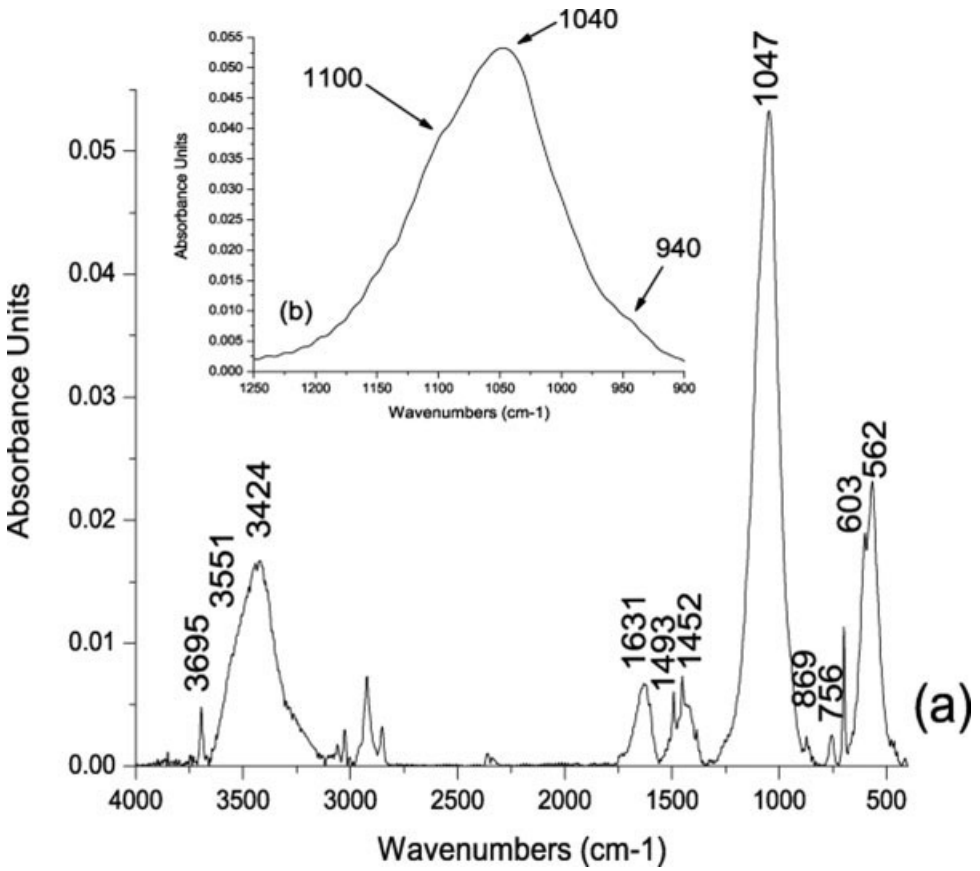

Figure 8. Infrared spectrum for the final calcium phosphate coating. (a) Full spectrum and (b) phosphate band only.

which are due to the PO_4^{3-} stretching vibrations.[45] Figure 8(b) shows the 1047 cm^{-1} phosphate band region of the spectrum in more detail. Upon closer inspection it is clear that this band has three components; the main peak centered at 1040 cm^{-1} and two shoulders at 940 and 1100 cm^{-1}. The weak shoulder at 940 cm^{-1} is the ν_1 symmetric P—O stretching mode.[47] This mode is IR-inactive in the free phosphate ion, but appears as a weak band due to a reduction in symmetry of the phosphate ion upon incorporation into the crystal lattice.[47] The ν_3 antisymmetric P—O stretching mode is triply degenerate in the free phosphate ion, but this mode is resolved into at least two distinct peaks in crystalline hydroxyapatite.[47] It has been shown that as the crystallinity of the hydroxyapatite increases these two ν_3 bands become increasingly resolved.[47] In our infrared spectrum, the two ν_3 bands are observed at 1040 and 1100 cm^{-1} However, they are poorly resolved, which indicates that the coating is only poorly crystalline.[47] This is not surprising since our XPS results have demonstrated that a significant amount of magnesium ions are incorporated into the coating itself, and magnesium ions are known to inhibit crystal growth in hydroxyapatite.[49] These two observations coupled together suggest that the hydroxyapatite coating formed is a calcium-deficient/magnesium-rich hydroxyapatite material.

XRD results

The XRD pattern for the coating is shown in Figure 9. This pattern indicates that there are likely two different compounds present in the sample, hydroxyapatite ($Ca_{10}(PO_4)_6(OH)_2$) and scholzite ($CaZn_2(PO_4)_2{\cdot}2H_2O$). The broad diffraction peaks

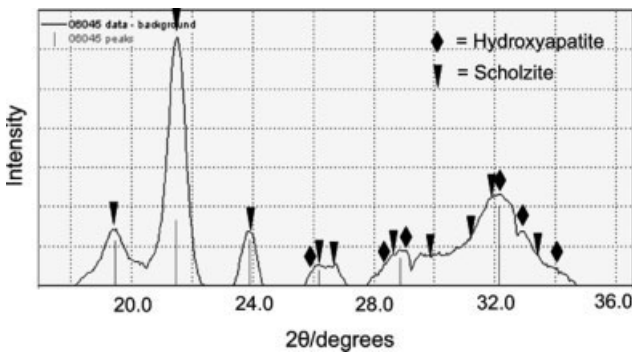

Figure 9. X-ray diffraction pattern for the final calcium phosphate coating.

indicate that both of these compounds are poorly crystalline, however, the intensity of the scholzite peaks suggest that this compound has improved crystallinity compared to the hydroxyapatite. Our XPS data indicate that the concentration of zinc in the coating is $\leq$1% therefore the increased intensity of the scholzite peaks must be due to the crystallinity of the compound and not an abundance of the material. The XRD pattern obtained is not typical of crystalline hydroxyapatite. However, the peaks we have attributed to hydroxyapatite very closely match published XRD patterns for calcium-deficient hydroxyapatite.[49] Our XPS results show that the Ca/P ratio in our coatings is ~1:1, this is much lower than the predicted Ca/P ratio of 1.67:1 for hydroxyapatite. This result indicates that our hydroxyapatite coating is calcium-deficient. We also know that there is a significant amount of magnesium incorporated into the coating which makes a calcium magnesium hydroxyapatite the most likely phase present. In fact, it has been previously observed that the substitution of magnesium ions into the crystal structure of hydroxyapatite significantly decreases the crystallinity of the material.[50]

Proposed mechanism of deposition

The mechanism of apatite deposition on the magnesium alloy substrate can be summarized by the following three reactions:

$$\text{Step 1} - \mathrm{Mg} \rightarrow \mathrm{Mg^{2+}} + 2e^- \text{ and}$$
$$2\mathrm{H_2O} + 2e^- \rightarrow \mathrm{H_2}\uparrow + 2\mathrm{OH^-}$$
$$\text{Step 2} - \mathrm{H_2PO_4^-} \rightarrow \mathrm{HPO_4^{2-}} \rightarrow \mathrm{PO_4^{3-}}$$
$$\text{Step 3} - (10-x)\mathrm{Ca^{2+}} + \mathrm{xMg^{2+}} + 6\mathrm{PO_4^{3-}} + 2\mathrm{OH^-} \rightarrow (\mathrm{Ca_{(10-x)}Mg_x})(\mathrm{PO_4})_6(\mathrm{OH})_2$$

Upon immersion of the substrate in the coating bath, the anodic dissolution of magnesium begins. This is evidenced by the increase in the concentration of magnesium in the bath and the observed increase in pH. Our XPS results reveal that there is an increase in the surface concentration of zinc in the early stages of deposition. The XRD spectrum confirms the presence of a small amount of calcium zinc phosphate (scholzite) in the coating material. Coupled together, these two results imply that the initial corrosion of the magnesium alloy substrate occurs at the interface between the α and β phases of the material, since zinc is associated primarily with the aluminium-rich β phase. It is likely that the anodic dissolution at these sites catalyzes the heterogeneous nucleation and growth of the calcium phosphate coating due to a local rise in pH.

Although the XRD and infrared results confirm that the coating is primarily hydroxyapatite, our XPS results reveal that the Ca/P ratio is less than that of stoichiometric HA. Furthermore, the coating is poorly crystalline and has been shown to contain significant amounts of magnesium. These results suggest that the magnesium ions are readily incorporated into the crystal lattice of the hydroxyapatite during the deposition of the coating. The composition of the final coating is primarily a magnesium-rich/calcium-deficient hydroxyapatite.

CONCLUSIONS

In this article, a solution chemistry technique for the deposition of calcium phosphate coatings on magnesium alloys has been reported. Kinetic studies of the deposition process have shown that the heterogeneous nucleation and growth of the calcium phosphate coating is catalyzed by anodic dissolution of the magnesium alloy substrate in the early stages of deposition. Characterization of the coating revealed that the primary phase formed is a poorly crystalline calcium magnesium hydroxyapatite material.

We thank Mr. Mark Biesinger of Surface Science Western for technical assistance with our X-ray photoelectron spectroscopy studies.

References

1. Ambrose CG, Clanton TO. Bioabsorbable implants: Review of clinical experience in orthopedic surgery. Ann Biomed Eng 2004;32:171–177.
2. Rokkanen PU, Bostman O, Hirvensalo E, Makela EA, Partio EK, Patiala H, Vainionpaa S, Vihtonen K, Tormala P. Bioabsorbable fixation in orthopaedic surgery and traumatology. Biomaterials 2000;21:2607–2613.
3. Bostman O, Pihlajamaki H. Clinical biocompatibility of biodegradable orthopaedic implants for internal fixation: A review. Biomaterials 2000;21:2615–2621.
4. Staiger MP, Pietak AM, Huadmai J, Dias G. Magnesium and its alloys as orthopedic biomaterials: A review. Biomaterials 2006;27:1728–1734.
5. Lindstrom R, Johansson LG, Svensson JE. The influence of NaCl and CO_2 on the atmospheric corrosion of magnesium alloy AZ91. Mater Corros 2003;54:587–594.
6. Inoue H, Sugahara K, Yamamoto A, Tsubakino H. Corrosion rate of magnesium and its alloys in buffered chloride solutions. Corros Sci 2002;44:603–610.
7. Song GL, Atrens A. Corrosion mechanisms of magnesium alloys. Adv Eng Mater 1999;1:11–33.
8. Zreiqat H, Evans P, Howlett CR. Effect of surface chemical modification of bioceramic on phenotype of human bone-derived cells. J Biomed Mater Res 1999;44:389–396.
9. Li L, Gao J, Wang Y. Evaluation of cyto-toxicity and corrosion behavior of alkali-heat-treated magnesium in simulated body fluid. Surf Coat Technol 2004;185:92–98.

10. Waksman R, Pakala R, Kuchulakanti PK, Baffour R, Hellinga D, Seabron R, Tio FO, Wittchow E, Hartwig S, Harder C, Rohde R, Heublein B, Andrea A, Waldmann KH, Haverich A. Safety and efficacy of bioabsorbable magnesium alloy stents in porcine coronary arteries. Catheter Cardiovasc Interv 2006;68:607–617.
11. Witte F, Ulrich H, Rudert M, Willbold E. Biodegradable magnesium scaffolds: Part I: Appropriate inflammatory response. J Biomed Mater Res A 2007;81:748–756.
12. Witte F, Ulrich H, Palm C, Willbold E. Biodegradable magnesium scaffolds: Part II: Peri-implant bone remodeling. J Biomed Mater Res A 2007;81:757–765.
13. Witte F, Feyerabend F, Maier P, Fischer J, Stormer M, Blawert C, Dietzel W, Hort N. Biodegradable magnesium-hydroxyapatite metal matrix composites. Biomaterials 2007;28:2163–2174.
14. Nandakumar K, Sreekumari KR, Kikuchi Y. Antibacterial properties of magnesium alloy AZ31B: in-vitro studies using the biofilm-forming bacterium Pseudomonas sp. Biofouling 2002;18:129–135.
15. Witte F, Kaese V, Haferkamp H, Switzer E, Meyer-Lindenberg A, Wirth CJ, Windhagen H. In-vivo corrosion of four magnesium alloys and the associated bone response. Biomaterials 2005;26:3557–3563.
16. Levesque J, Dube D, Fiset M, Mantovani D. Investigation of corrosion behaviour of magnesium alloy AM60B-F under pseudo-physiological conditions. Mater Sci Forum 2003;426: 521–526.
17. Waksman R, Pakala R, Hellinga D. Effect of bioabsorbable magnesium alloy stent on neointimal formation in a porcine coronary model. Eur Heart J 2005;26:417.
18. Liu CL, Xin YC, Tang GY, Chu PK. Influence of heat treatment on degradation behavior of bio-degradable AZ63 magnesium alloy in simulated body fluid. Mater Sci Eng A 2007; 456:350–357.
19. Song GL. Control of biodegradation of biocompatible magnesium alloys. Corros Sci 2007;49:1696–1701.
20. Liu CG, Xin YC, Tian XB, Zhao J, Chu PK. Corrosion resistance of titanium ion implanted AZ91 magnesium alloy. J Vac Sci Technol A 2007;25:334–339.
21. Hench LL, Best S. Ceramics, glasses and glass-ceramics. In: Ratner B, Hoffman A., Schoen FJ, Lemons JE, editors. Biomaterials Science: An Introduction to Material in Medicine. London: Elsevier Academic Press; 2004. p 165–167.
22. Dorozhkin SV, Epple M. Biological and medical significance of calcium phosphates. Angew Chem 2002;41:3130–3146.
23. Puleo DA, Nanci A. Understanding and controlling the bone-implant interface. Biomaterials 1999;20:2311–2321.
24. Chakraborty J, Sinha M, Basu K. Biomolecular template-induced biomimetic coating of hydroxyapatite on an SS 316L substrate. J Am Ceram Soc 2007;90:1258–1261.
25. Zhang E, Yang K. Biomimetic coating of calcium phosphate on biometallic materials. Trans Nonferrous Met Soc China 2005;15:1199–1205.
26. Li F, Feng Q, Cui F, Li H, Schubert H. A simple biomimetic method for calcium phosphate coating. Surf Coat Technol 2002;154:88–93.
27. Zhang Q, Leng Y. Electrochemical activation of titanium for biomimetic coating of calcium phosphate. Biomaterials 2005; 26:3853–3859.
28. Du C, Klasens P, Haan RE, Bezemer J, Cui FZ, deGroot K, Layrolle P. Biomimetic calcium phosphate coatings on Polyactive 1000/70/30. J Biomed Mater Res 2002;59:535–546.
29. Kumar M, Xie J, Chittur K, Riley C. Transformation of modified brushite to hydroxyapatite in aqueous solution: Effects of potassium substitution. Biomaterials 1999;20:1389–1399.
30. Barrere F, van Blitterswijk CA, deGroot K, Layrolle P. Nucleation of biomimetic Ca-P coatings on Ti6Al4V from a SBFx5 solution: Influence of magnesium. Biomaterials 2002;23:2211–2220.
31. Lin FH, Hsu YS, Lin SH, Chen TM. The growth of hydroxyapatite on alkaline treated Ti-6Al-4V soaking in higher temperature with concentrated Ca2+/HPO4- simulated body fluid. Mater Chem Phys 2004;87:24–30.
32. Pecheva E, Pramatoaova L, Maitz M, Pham MT, Kondyuirin AV. Kinetics of hydroxyapatite deposition on solid substrates modified by sequential implantation of Ca and P ions Part II: Morphological, composition and structure study. Appl Surf Sci 2004;235:170–175.
33. Ribeiro C, Rigo ECS, Sepulveda P, Bressiani JC, Bressiani AHA. Formation of calcium phosphate layer on ceramics with different reactivities. Mater Sci Eng C 2004;24:631–636.
34. Wan YZ, Juang Y, He F, Wang YL, Zhao ZG, Ding HF. Effect of Mg ion implantation on calcium phosphate formation on titanium. Surf Coat Technol 2006;201:2904–2909.
35. Kuwahara H, Al-Abdullat Y, Ohta M, Tsutsumi S, Ikeuchi K, Mazaki N, Aizawa T. Surface reaction of magnesium in Hank's solution. Magnesium Alloys 2000;350:349–358.
36. Ghali E, Dietzel W, Kainer KU. General and localized corrosion of magnesium alloys: A critical review. J Mater Eng Perform 2004;13:7–23.
37. Harris DC. Quantitative Chemical Analysis. New York: W. H. Freeman and Company; 2003. p AP20.
38. Verestiuc L, Morosanu C, Bercu M, Pasuk I, Mihailescu IN. Chemical growth of calcium phosphate layers on magnetron sputtered HA films. J Cryst Growth 2004;264:483–491.
39. Zhang Q, Chen J, Feng J, Cao Y, Deng C, Zhang X. Dissolution and mineralization behaviours of HA coatings. Biomaterials 2003;24:4741–4748.
40. Ambat R, Zhou W. Electroless nickel-plating on AZ91D magnesium alloy: Effect of substrate microstructure and plating parameters. Surf Coat Technol 2004;179:124–134.
41. Fotea C, Callaway J, Alexander MR. Characterization of the surface chemistry of magnesium exposed to the ambient atmosphere. Surf Int Anal 2006;38:1363–1371.
42. Rotole JA, Sherwood PMA. Oxide-free phosphate surface films on metals studied by core and valence band X-ray photoelectron spectroscopy. Chem Mater 2001;13:3933–3942.
43. Felker DL, Sherwood PMA. Magnesium phosphate (Mg3(PO4)2) by XPS. Surf Sci Spec 2002;9:83–90.
44. Lu HB, Campbell CT, Graham DJ, Ratner BD. Surface characterization of hydrxoyapatite and related calcium phosphates by XPS and TOF-SIMS. Anal Chem 2000;72:2886–2894.
45. Yu S, Hariram KP, Kumar R, Cheang P, Aik KK. In vitro apatite formation and its growth kinetics on hydroxyapatite/polyetheretherketone biocomposites. Biomaterials 2005;26:2343–2352.
46. Antonakos A, Liarokapis E, Leventouri T. Micro-Raman and FTIR studies of synthetic and natural apatites. Biomaterials 2007;28:3043–3054.
47. Pleshko N, Boskey A, Mendelsohn R. Novel infrared spectroscopic method for the determination of crystallinity of hydroxyapatite minerals. Biophys J 1991;60:786–793.
48. Frost RL. An infrared and Raman spectroscopic study of natural zinc phosphates. Spectrochim Acta 2004;60:1439–1445.
49. Meneghini C, Dalconi MC, Nuzzo S, Mobilio S, Wenk RH. Rietveld refinement on X-ray diffraction patterns of bioapatite in human fetal bones. Biophys J 2003;84:2021–2029.
50. Yasukawa A, Ouchi S, Kandori K, Ishikawa T. Preparation and characterization of magnesium-calcium hydroxyapatites. J Mater Chem 1996;6:1401–1405.